CHEMISTRY OF MATERIALS
Article

Chem. Mater. **2010,** *22,* 2347–2356 2347
DOI:10.1021/cm903573a

Structure and Properties of Noncrystalline Aluminum Oxide-Hydroxide Fluorides

Christoph Stosiek,[†] Gudrun Scholz,[†] Sven L. M. Schroeder,[‡] and Erhard Kemnitz*,[†]

[†]*Institut für Chemie, Humboldt-Universität zu Berlin Brook-Taylor-Strasse 2, D-12489 Berlin, Germany, and* [‡]*School of Chemical Engineering an Analytical Science, The University of Manchester P.O. Box 88, Manchester, M60 1QD, U.K.*

Received November 25, 2009. Revised Manuscript Received February 12, 2010

The thermal treatment of sol−gel derived aluminum hydroxide fluorides leads to new, X-ray amorphous, macroporous aluminum oxide-hydroxide fluorides. Followed by EA, DTA-TG, XPS, FT-IR, NH_3-TPD, BET, XRD, and MAS NMR, it can be shown that the simplified composition of these compounds is "AlFO" and "$AlF_2O_{1/2}$", respectively. These aluminum oxide-hydroxide fluorides exhibit a large number of acid centers. The local structure consists of AlF_xO_{cn-x} units (cn, coordination numbers 6, 5, 4), and all sites are partially fluorinated. It can be shown that bridged and terminal F-sites are related to 5- and 6-fold coordinated Al sites.

Introduction

Aluminum hydroxide fluorides (e.g., pyrochlore) are well-known compounds with high surface areas, particle sizes in the nanoscale range, and strong Lewis acid sites as well as weak and medium strong Brønsted sites.[1] These properties make aluminum hydroxide fluorides valuable catalysts in, e.g., the synthesis of α-tocopherol (vitamin E),[2] halogen exchange reactions,[3] or Friedel−Crafts acylation.[4] Such aluminum hydroxide fluorides can be synthesized by many ways, e.g., by precipitation from solutions of aluminum fluorosulfate by treatment with ammonia[5] or thermal treatment of $AlF_2(O^tBu)$.[6] In order to obtain compounds with a tunable OH/F molar ratio, other more versatile synthesis routes have to be used. An appropriate synthesis route is the microwave-assisted synthesis of crystalline aluminum hydroxide fluorides in pyrochlore structure as developed by Dambournet et al.[7,8] The thermal treatment of such crystalline phases leads to a decomposition into aluminum fluoride and oxide.[9,10] Therefore, the synthesis of amorphous aluminum oxide-hydroxide fluorides by thermal treatment of the crystalline compounds is not successful. As published recently, a new synthesis route to X-ray amorphous aluminum hydroxide fluorides was established according a fluorolytic sol−gel synthesis using aqueous hydrofluoric acid as the fluorinating agent.[11] The thermal treatment of such samples results in the loss of water and therefore the formation of aluminum oxide-hydroxide fluoride phases (see eq 1). Regarding their formal composition, these are the first noncrystalline aluminum oxide fluorides known so far. In literature, two crystalline aluminum oxide fluorides with different crystal structures are known. In 1992, Kutoglu described the rutile structure of tetragonal AlFO, which was obtained as an unexpected byproduct in the synthesis of complex oxides in PbF-melts.[12] Recently, Vasiliev et al. reported on orthorhombic AlFO, also obtained as an unexpected byproduct in the $SrAlF_5$ synthesis.[13] The crystal structure contains $Al(F/O)_4$ tetrahedra and $Al(F/O)_6$ octahedra. Both structural units are partially fluorinated. Terminal fluorine sites only occur on the 6-fold coordinated aluminum species.

It is the intention of the present contribution to study structure and properties of noncrystalline aluminum oxide-hydroxide fluorides isolated after quenching aluminum hydroxide fluorides at 300 and 500 °C, respectively. Subsequently these samples were handled under inert conditions.

Structural information was derived applying solid state NMR (^{27}Al, ^{29}F), FT-IR, and XPS spectroscopies. Properties, such as BET surface areas, pore sizes, and

*Corresponding author. Prof. Dr. Erhard Kemnitz, fax: +49 (0)30 2093 7277. E-mail: erhard.kemnitz@chemie.hu-berlin.de.

(1) Dambournet, D.; Demourgues, A.; Martineau, C.; Durand, E.; Majimel, J.; Vimont, A.; Leclerc, H.; Lavalley, J.-C.; Daturi, M.; Legein, C.; Buzaré, J.-Y.; Fayone, F.; Tressaud, A. *J. Mater. Chem.* **2008**, *18*, 2483–2492.
(2) Coman, S. M.; Wuttke, S.; Vimont, A.; Daturi, M.; Kemnitz, E. *Adv. Synth. Catal.* **2008**, *350*, 2517.
(3) Kemnitz, E.; Menz, D. H. *Prog. Solid State Chem.* **1998**, *26*, 97.
(4) Moreno-Bravo, M.; Hernandez-Luna, M.; Alcaraz-Cienfuegos, J.; Rosas-Aburto, A. *Appl. Catal., A* **2003**, *249*, 35.
(5) Cowley, J. M.; Scott, T. R. *J. Am. Chem. Soc.* **1948**, *70*, 105.
(6) Johnson, R. L.; Siegel, B. *Nature* (*London, U.K.*) **1966**, *210*, 1256.
(7) Dambournet, D.; Demourgues, A.; Martineau, C.; Durand, E.; Majimel, J.; Legein, C.; Buzare, J. Y.; Fayon, F.; Vimont, A.; Leclerc, H.; Tressaud, A. *Chem. Mater.* **2008**, *20*, 7095.
(8) Dambournet, D.; Demourgues, A.; Martineau, C; Pechev, S.; Lhoste, J.; Majimel, J.; Vimont, A.; Lavalley, J.-C.; Legein, C.; Buzaré, J.-Y.; Fayon, F.; Tressaud, A. *Chem. Mater.* **2008**, *20*, 1459.
(9) Menz, D.; Mensing, Ch.; Hönle, W.; von Schnering, H. G. *Z. Anorg. Allg. Chem.* **1992**, *611*, 107.
(10) Menz, D.; Zacharias, A.; Kolditz, L. *J. Therm. Anal.* **1988**, *33*, 811.
(11) Stosiek, Ch.; Scholz, G.; Eltanany, G.; Bertram, R.; Kemnitz, E. *Chem. Mater.* **2008**, *20*, 5687.
(12) Kutoglu, A. *Z. Kristallogr.* **1992**, *199*, 197.
(13) Vasiliev, A. D.; Melnikova, S. V.; Isaenko, L. I. *Acta Crystallogr., Sect. C: Cryst. Struct. Commun.* **2009**, *65*, i20.

Published on Web 02/26/2010

strengths of acid sites as well as their rehydration behavior were the focus of interest.

Experimental Section

The procedure for the preparation of the aluminum hydroxide fluorides is given in ref 11. For the thermal dehydration experiments presented here, we selected two of the samples, namely, $AlF_{0.9}(OH)_{2.1}$ (designated as $AlF(OH)_2$) and $AlF_{2.1}(OH)_{0.9}$ (designated as $AlF_2(OH)$).

The dehydration of $AlF(OH)_2$ and $AlF_2(OH)$ was performed in a tube furnace in flowing argon (20 mL/min). To ensure quasi-equilibrium conditions of the solid with its own gaseous atmosphere, the thermal treatment was performed in a Q-crucible. The samples were heated (heating rate 5 °C/min) to a temperature of 300 °C (designated as $AlF_x(OH)_y$-300) or rather 500 °C (designated as $AlF_x(OH)_y$-500). The dwell time at these temperatures was 4 h. The aluminum oxide-hydroxide fluorides are moisture sensitive and were stored in a glovebox under argon atmosphere.

For X-ray powder diffraction measurements, a Seifert XRD 3003 TT equipment (Freiberg, Germany) with CuKα radiation was applied. The moisture-sensitive samples were prepared in a glovebox and covered with Kapton-foil.

Thermal analysis experiments were performed on a STA 409 C (Netzsch Gerätebau GmbH, Selb, Germany) equipped with a quadrupole mass spectrometer Balzers QMG 422. A DTA-TG sample-holder system (Pt/PtRh10 thermocouple) was used. Measurements were performed in N_2 atmosphere.

The temperature programmed desorption of ammonia (NH_3-TPD) was used to characterize the strength of the acid sites and their distribution in the solids.[14] The samples were pretreated at 250 °C for 1 h. Afterward, ammonia was adsorbed onto the surface of the samples at room temperature. Ammonia desorption was monitored during TPD (10 °C/min up to 500 °C) by FT-IR detection of the band at 930 cm^{-1} (FT-IR system 2000, Perkin-Elmer). The total amount of desorbed ammonia was determined by reaction with an excess of sulfuric acid and back-titration with sodium hydroxide solution.

FT-IR spectra of KBr pellets were recorded on a Perkin-Elmer 2000 spectrometer in transmission mode. About 250 mg of KBr (Fluka, Germany) was pressed with 1.0−1.5 mg of the sample, and then the samples were measured in the regions 5000−400 cm^{-1}.

XPS measurements were performed with a KRATOS Axis Ultra system. The equipment is fitted with a monochromatized AlKα X-ray source, an aspherical mirror electron analyzer, and a charge neutralization system. Before recording the spectra, the samples were stored in a vacuum of better than 1×10^{-6} mbar in order to degas. During the measurement, the vacuum in the spectrometer was better than 1×10^{-8} mbar. High-resolution scans of the emission features (Al 2p, F 1s, O 1s) were taken on an energy grid of 0.1 eV and with a pass energy of 20 eV. The analysis of the data was carried out using CasaXPS (Casa Software, U.K.). The C 1s emission from adventitious carbon at 284.8 eV was used as the binding energy reference.

MAS NMR spectra were recorded at spinning speeds of 25 and 30 kHz and resonance frequencies of 376.4 MHz for ^{19}F and 104.6 MHz for ^{27}Al on a Bruker AVANCE 400 spectrometer equipped with a 2.5 mm MAS probe. ^{19}F MAS NMR ($I = 1/2$) spectra were recorded with a $\pi/2$ pulse duration of p1 = 2 μs, a spectrum width of 400 kHz, a recycle delay of 10 s, and an accumulation number of 64. Isotropic chemical shifts of ^{19}F are given with respect to the $CFCl_3$ standard. Background signals of ^{19}F could be completely suppressed with the application of a phase-cycled depth pulse sequence according to Cory and Ritchey.[15] In addition, ^{19}F rotor-synchronized delayed echo experiments were performed at ν_{rot} = 25 kHz utilizing different spin−spin relaxation times (T_2) of different species.

^{27}Al MAS NMR ($I = 5/2$) spectra were recorded with an excitation pulse duration of 1 μs. A 1 M aqueous solution of $AlCl_3$ was used as reference for the chemical shift of ^{27}Al. The recycle delay was chosen as 1 s, and the accumulation number was 20 000 if not otherwise given.

For $^{19}F \rightarrow {}^{27}Al$ CP MAS NMR experiments, a contact time of 700 μs was used (ν_{rot} = 25 kHz). In preparation for the $^{19}F-{}^{27}Al$ heteronuclear correlation (HETCOR) experiments (based on wideline separation (WISE) procedure), the cross polarization (CP) conditions at ν_{rot} = 25 kHz were optimized for each sample for the rf field of the ^{27}Al nucleus (expressed as powder level pl1).

^{27}Al triple quantum MAS NMR spectra were achieved using a three pulse *z*-filter sequence. For the creation of the 3Q-coherence, a pulse with a duration of 3.5 μs and for the conversion (±3Q → 0Q) a pulse with a duration of 1.5 μs, both at a rf field strength of 125 kHz, were applied. The selective *z*-filter pulse lasted for 8 μs (rf field, 13 kHz). After a two-dimensional Fourier transformation, the spectra were sheared, resulting in pure absorption mode 2D contour plots.[16]

Simulation of the spectra was performed with the DMFIT program in its actual version.[17] The starting values were achieved from the 3Q MAS NMR spectra as described below. The results of the simulations are summarized in Table 2.

Elemental analyses (EA) of the samples were performed with a LECO CHNS-932 combustion equipment (C, H, N). The fluoride contents were determined with a fluoride sensitive electrode after conversion of the solids with Na_2CO_3/K_2CO_3 into a soluble form. The aluminum contents of the samples were determined by ICP OES (IRIS Intrepid HR DUO) after a microwave assisted (ETHOS plus) conversion with a H_3PO_4/HNO_3 mixture into a soluble form. The instrument was calibrated with standard solution.

The surface areas of the samples were determined using Ar adsorption by means of a micromeritics ASAP 2020 instrument at −196 °C. Before each measurement, the samples were degassed at 5×10^{-5} mbar and 150 °C for 12 h. The isotherms were processed by Brunauer−Emmett−Teller (BET) models.

Results and Discussion

The elemental composition, the specific surface area, the porosity type, and the average pore diameter of the different samples are summarized in Table 1. As expected, the thermal treatment not only leads to a release of water but also to changes in the sample morphology. Surface areas decrease and the pore type changes from meso- to macroporous, accompanied by an increase of the average pore diameter (see Table 1). The thermoanalytic plots of

(14) Quaschning, V.; Deutsch, J.; Druska, P.; Niclas, H. J.; Kemnitz, E. *J. Catal.* **1998**, *177*, 164.

(15) Cory, D. G.; Ritchey, W. M. *J. Magn. Reson.* **1988**, *80*, 128.

(16) König, R.; Scholz, G.; Kemnitz, E. *J. Phys. Chem. C* **2009**, *113*, 6426.

(17) Massiot, D.; Fayon, F.; Capron, M.; King, I.; Le Calve, S.; Alonso, B.; Durand, J. O.; Bujoli, B.; Gan, Z. H.; Hoatson, G. *Magn. Reson. Chem.* **2002**, *40*, 70.

Table 1. Sample Composition, BET Surface Area, Porosity Type, and Pore Diameter of Aluminum Oxide-Hydroxide Fluorides

sample name	Al (wt %)	F (wt %)	H (wt %)[a]	avg composition	surface area (m^2/g)	pore type	avg pore diameter (Å)
$AlF(OH)_2$	33.9 ± 0.8	22.7 ± 2	2.6 ± 1	$AlF_{0.9}(OH)_{2.1}$	495	mesoporous	30
$AlF(OH)_2$-300	37.1 ± 0.8	24.1 ± 2	0.6 ± 2	$AlF_{0.9}(OH)_{1.1}O_{0.5}$	154	macroporous	150
$AlF_2(OH)$	31.2 ± 0.7	45.3 ± 2	1.4 ± 1	$AlF_{2.1}(OH)_{0.9}$	502	mesoporous	90
$AlF_2(OH)$-300	33.8 ± 0.8	41.7 ± 2	0.9 ± 2	$AlF_{1.8}(OH)_{0.8}O_{0.2}$	133	macroporous	300

[a] The measuring accuracy is limited for hydrogen due to H content near the detection limit.

Table 2. Centers of Gravity (δ_{3QMAS}, δ_{MAS}) of the 2D Line Shapes for Different Al Sites and Resulting Data for the Quadrupolar Product and Isotropic Chemical Shift Compared with Data Obtained by Simulation Applying Czjzek-Distribution Functions[a]

sample		species	δ_{3QMAS}	δ_{MAS}	δ_{iso}	$\nu_{Q\eta}$	fwhm	%
		Al6-1	6.8	−5.4	2.2	558		
		Al6-2	10.1	−13.3	1.4	775		
		Al6-3	21.69	−21.56	5.7	1054		
	3Q MAS	Al5-1	43.4	26.6	37.2	656		
		Al4-1	73.2	56.8	67.2	649		
		Al4-2	81.0	41.7	66.4	1003		
$AlF(OH)_2$-300								
		Al6-1			1.8	579	19	21.9
		Al6-2			−9.3	1151	5	21.7
	simulation	Al6-3			14.1	687	17	7.5
		Al5-1			34.8	649	19	13.2
		Al4-1			70.3	1141	14	23.6
		Al4-2			66.5	964	85	12.1
		Al6-1	0.0	−11.2	−4.1	535		
		Al6-2	−8.7	−18.0	−12.1	489		
	3Q MAS	Al6-3	19.2	11.5	16.4	444		
		Al5-1	37.1	22.7	31.8	609		
		Al4-1	70.4	57.9	65.8	565		
$AlF_2(OH)$-300								
		Al6-1			−3.4	506	19	38.4
		Al6-2			−8.6	1046	5	32.7
	simulation	Al6-3			15.8	464	14	5.5
		Al5-1			31.6	543	19	5.6
		Al4-1			65.4	926	46	17.8

[a] $\nu_{Q\eta}$, quadrupolar product in kHz; fwhm, full width at half maximum of the isotropic chemical shift gaussian distribution; %, relative intensity; δ_{3QMAS}, δ_{MAS}, δ_{iso}, and fwhm are all in parts per million (ppm).

$AlF(OH)_2$ and $AlF_2(OH)$ (parts a and c of Figure 1, TG curve) consist of two steps. In both cases, the mass loss of the first step corresponds very well with the mass loss caused by dehydration. The application of differential thermoanalysis discloses for, e.g., $AlF(OH)_2$, a mass loss of 25.6% in a wide temperature range between 25 and 900 °C (see Figure 1a). This mass loss can be mainly assigned to the water release. Following the simplified equation

$$AlF(OH)_2 \rightarrow AlFO + H_2O \qquad (1)$$

the theoretical mass loss is with 22.5% a bit lower than the experimental value, which can be rationalized by the generation of HF due to hydrolysis effects. The dehydration leads to strongly disordered, X-ray amorphous aluminum oxide-hydroxide fluorides which can be formally described by a mean formula of "AlFO" and "$AlF_2O_{1/2}$", respectively. These findings are in agreement with the results of the elemental analysis of $AlF(OH)_2$-300, $AlF(OH)_2$-500, $AlF_2(OH)$-300, and $AlF_2(OH)$-500 (Table 1). The release of water goes along with an increase of the relative amount of Al and F and with a decrease of the relative amount of H. After the thermal treatment at 300 °C, the samples not only lose water but also fluorine (as HF) because of the pyrohydrolysis.[11] The removal of OH groups from the samples leads to a strong rearrangement of their structure because of the formation of under-coordinated Al ions and the absence of some hydrogen bonds. Especially the under-coordinated Al ions are the reason for the very strong (Lewis) acid sites. The NH_3-TPD curves of $AlF(OH)_2$-300 and $AlF_2(OH)$-300 (Figure 1b and d) unambiguously illustrate the presence of acid sites in these samples. Both curves show two distinct maxima of ammonia desorption at ~200 °C and ~375 °C, which indicate moderate (200 °C) and very strong (375 °C) acidic centers.[18,19] Because of the handling of these samples, the acid centers should be predominantly characterized by Lewis acidity.

Beside differential thermoanalysis, the dehydration of the samples is also verified by FT-IR spectroscopy. In Figure 2, the FT-IR spectra of $AlF(OH)_2$ and $AlF_2(OH)$ calcined at 180 °C, 300 °C, and 500 °C are shown. For comparative purposes, the FT-IR spectrum of $AlF_x(OH)_{3-x}\cdot H_2O$ (pyrochlore) is shown in addition.

(18) Krahl, T. Amorphes Aluminiumchlorofluorid und -bromofluorid−die stärksten bekannten festen Lewis-Säuren. Doctoral Thesis, Humboldt-Universität zu Berlin, Berlin, Germany, **2005**.
(19) Murthy, J. K.; Gross, U.; Rudiger, S.; Rao, V. V.; Kumar, V. V.; Wander, A.; Bailey, C. L.; Harrison, N. M.; Kemnitz, E. *J. Phys. Chem. B* **2006**, *110*, 8314.

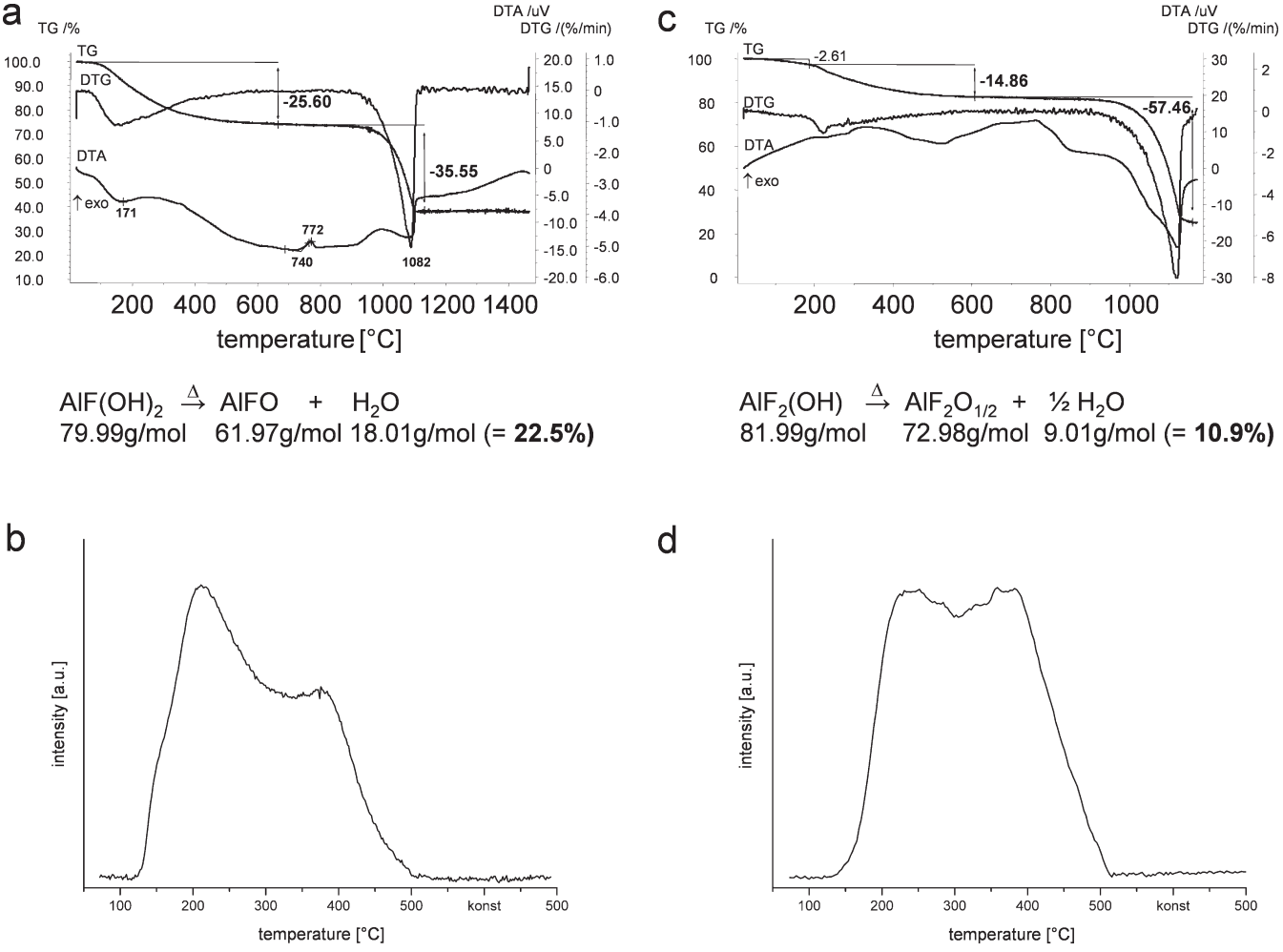

Figure 1. Thermoanalytic plots of $AlF(OH)_2$ (a) and $AlF_2(OH)$ (c) and temperature programmed desorption of ammonia (NH_3-TPD) of $AlF(OH)_2$-300 (b) and $AlF_2(OH)$-300 (d).

Broad vibration bands, obviously covering the ν_{OH} bands of different species (OH, H_2O), make an unambiguous interpretation difficult. With increasing temperature, the intensities of the OH stretching vibration bands (~3400 cm^{-1}) and the typical band of the deformation vibration of water (~1600 cm^{-1}) decrease.[8,20] The deformation vibration of Al−OH−Al-groups involved in hydrogen bridges to H_2O molecules is visible at about ~1100 cm^{-1}, which is very pronounced in the pyrochlore compound (Figure 2).[8,20] The spectrum of $AlF(OH)_2$-180 shows a very broad band at around 650 cm^{-1} which can be assigned to stretching and bending vibrations of different $AlF_{6-x}O_x$ octahedra. The band of the stretching vibration of Al−O at around 830 cm^{-1} is very intense and suggests a high amount of oxygen in the $Al(F/O)_6$ units present in the sample. Because of the high degree of disorder in the sample, the band of the bending vibrations at 1100 cm^{-1} is broad and the peak maximum is shifted compared to pyrochlore. After thermal treatment of $AlF(OH)_2$ at 300 °C, the bands indicating OH groups (~3500, 1100, and 830 cm^{-1}) and water (1600 cm^{-1}) become less intensive whereas intensities of the remaining bands are nearly

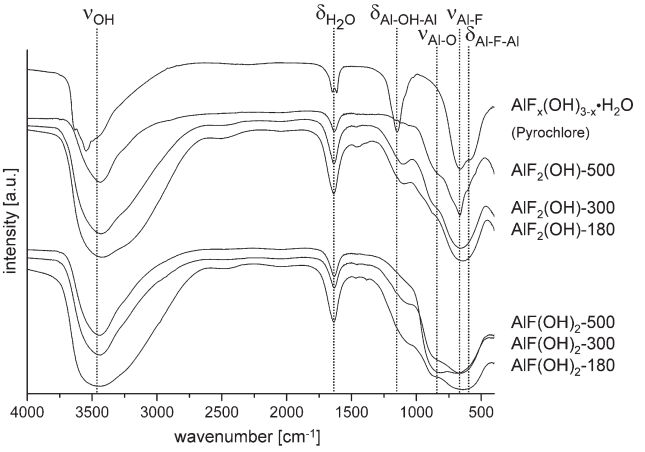

Figure 2. FT-IR spectra of aluminum hydroxide-fluoride in the pyrochlore structure, $AlF_x(OH)_{3-x}\cdot H_2O$ (for comparative purposes), AlF_2-(OH)-500, $AlF_2(OH)$-300, $AlF_2(OH)$-180, $AlF(OH)_2$-500, $AlF(OH)_2$-300, and $AlF(OH)_2$-180.

unchanged. In the spectrum of $AlF(OH)_2$-500, the OH and water bands are once again less intense than in the spectrum of $AlF(OH)_2$-300. Especially the intensity of the Al−OH−Al bending vibration is decreased in comparison with the vibrations of Al−F. The thermal treatment of the sample at 500 °C leads, as well as the thermal

(20) Vimont, A.; Lavalley, J. C.; Francke, L.; Demourgues, A.; Tressaud, A.; Daturi, M. *J. Phys. Chem. B* **2004**, *108*, 3246.

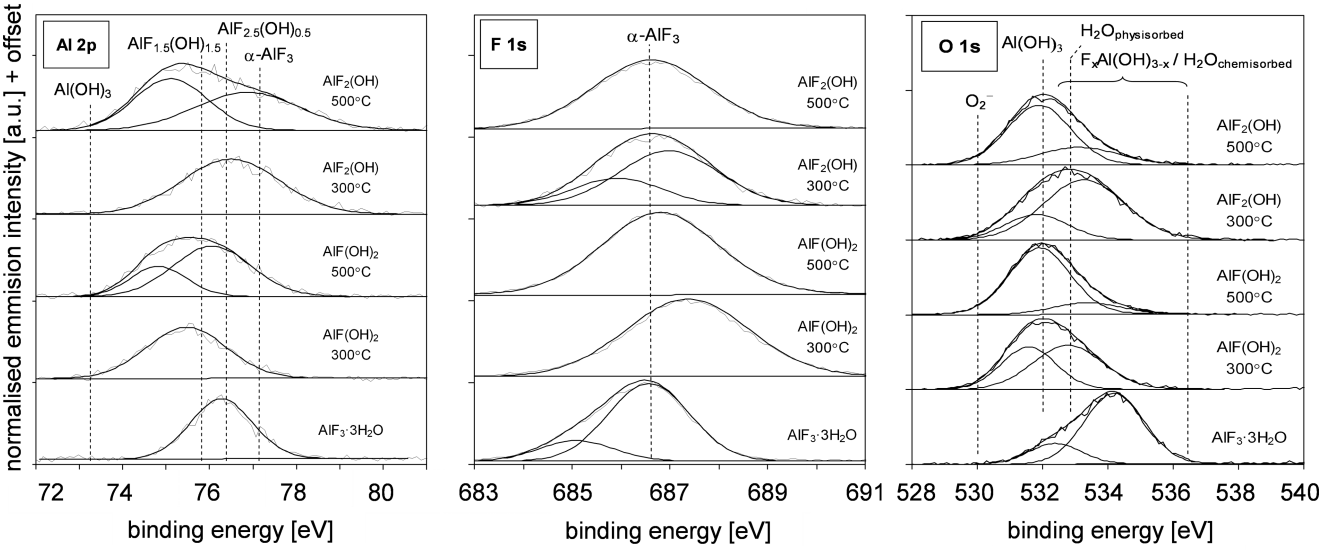

Figure 3. Al 2p, F 1s, and O 1s XPS spectra of $AlF_2(OH)$-500, $AlF_2(OH)$-300, $AlF(OH)_2$-500, $AlF(OH)_2$-300, and $AlF_3 \cdot 3H_2O$ (for comparative purposes).

treatment at 300 °C, to an increase of the structural order, visible at the narrower band of the Al−F−Al bending vibrations around 600 cm^{-1}. Because of the measurement settings, the samples were handled on air. That is the reason why intense water signals remain even after the thermal treatment. Following the rehydration behavior on air, it was found that within 1 h the samples absorb 1 mol % water when lying under air.

The shapes of all FT-IR spectra of $AlF_2(OH)$ are very similar to that of pyrochlore (Figure 2). Because of the, compared to $AlF(OH)_2$ samples, reduced amount of OH-groups, the intensity of the Al−O stretching vibrations is less intensive. Even the FT-IR spectrum of $AlF_2(OH)$-180 only shows a small shoulder at 830 cm^{-1}. The band of the stretching and bending vibrations of the $AlF_{6-x}O_x$ octahedra (~650 cm^{-1}) is narrower than in the sample $AlF(OH)_2$-180, which is a hint of a slightly higher structural order of the sample. This finding is supported by the narrower band of the Al−OH−Al bending vibration (~1100 cm^{-1}),[8,20] which is caused by a lesser distribution of the Al−OH−Al bonding angles. Thermal treatment of the sample at 300 °C leads to an intensity reduction of the OH and H_2O bands. The structural order of $AlF_2(OH)$-300 is higher than in AlF_2-(OH)-180, visible by a comparison of the broadness of the $\delta_{Al-OH-Al}$, ν_{Al-F}, and $\delta_{Al-F-Al}$ vibrations (Figure 2). Again, calcination at 500 °C leads to an enhanced dehydration of the sample. The intensity of the bands at around 3500 and 1600 cm^{-1} is reduced, and the Al−OH−Al bending vibration is nearly vanished.[8,20] $AlF_2(OH)$-500 has the highest ordered structure, visible at the relative small band at 650 cm^{-1}. Nevertheless, all samples are noncrystalline and therefore X-ray amorphous.

The surface composition of the samples was determined by X-ray photoelectron spectroscopy. Crystalline $AlF_3 \cdot 3H_2O$, α-AlF_3,[21,22] $Al(OH)_3$,[23] the HTB phase $AlF_{2.5}(OH)_{0.5}$,[22,24] and the pyrochlore structure $AlF_{1.5}(OH)_{1.5}$[22,24] were used as reference systems for comparison in all XPS measurements. The Al 2p spectrum of $AlF(OH)_2$-300 consists of a broad line with a maximum compatible with the stoichiometry $AlF(OH)_2$ (see Figure 3).[23] Strong broadening of the emission line (compared, for example, to the spectrum of stoichiometric $AlF_3 \cdot 3H_2O$) indicates that the phase contains a range of Al species with different local chemical environments, in agreement with the results of the NMR measurement. It seems unlikely that the local structure of the $AlF(OH)_2$ phase resembles those in either the HTB or the pyrochlore reference phases, because the F 1s binding energy is overall significantly higher. Especially the center of the F 1s emission from $AlF(OH)_2$-300 shows an unusually high binding energy of 687.5 eV,[23] which is similar to that observed previously for a noncrystalline product obtained by thermal dehydration of an amorphous sol−gel-derived hydrated $AlF_{2.3}(OH)_{0.7}$ precursor.[24] In agreement with the Al 2p spectrum, a broadened single line is detected, indicating a range of species with different electronic structure. The O 1s spectrum of $AlF(OH)_2$-300 can be interpreted as two groups of O species: O(H) groups similar to AlO_6 units as in AlO(OH) (531.5 eV)[23,25] or Al_2O_3 (531.6 eV)[23,26] and OH species that are presumably geminal to fluorine. After calcination at 500 °C, the maximum of the Al 2p spectrum of $AlF(OH)_2$-500 is shifted to higher binding energy, because the relative content of electronegative fluorine and oxide raise as a consequence of dehydration. The deconvolution

(21) König, R.; Scholz, G.; Scheurell, K.; Heidemann, D.; Buchem, I.; Unger, W. E. S.; Kemnitz, E. *J. Fluorine Chem.* **2010**, *131*, 91.
(22) Boese, O.; Unger, W. E. S.; Kemnitz, E.; Schroeder, S. L. M. *Phys. Chem. Chem. Phys.* **2002**, *4*, 2824.
(23) Böse, O.; Kemnitz, E.; Lippitz, A.; Unger, W. E. S. *Fresenius' J. Anal. Chem.* **1997**, *358*, 175.
(24) Makarowicz, A. Surface Characterisation of Functionalised Fluoride Materials. Ph.D. Thesis, The University of Manchester, Manchester, U.K., **2007**.
(25) Taylor, J. A. *J. Vac. Sci. Technol.* **1982**, *20*, 751.
(26) Tan, B. J.; Klabunde, K. J.; Sherwood, P. M. A. *J. Am. Chem. Soc.* **1991**, *113*, 855.

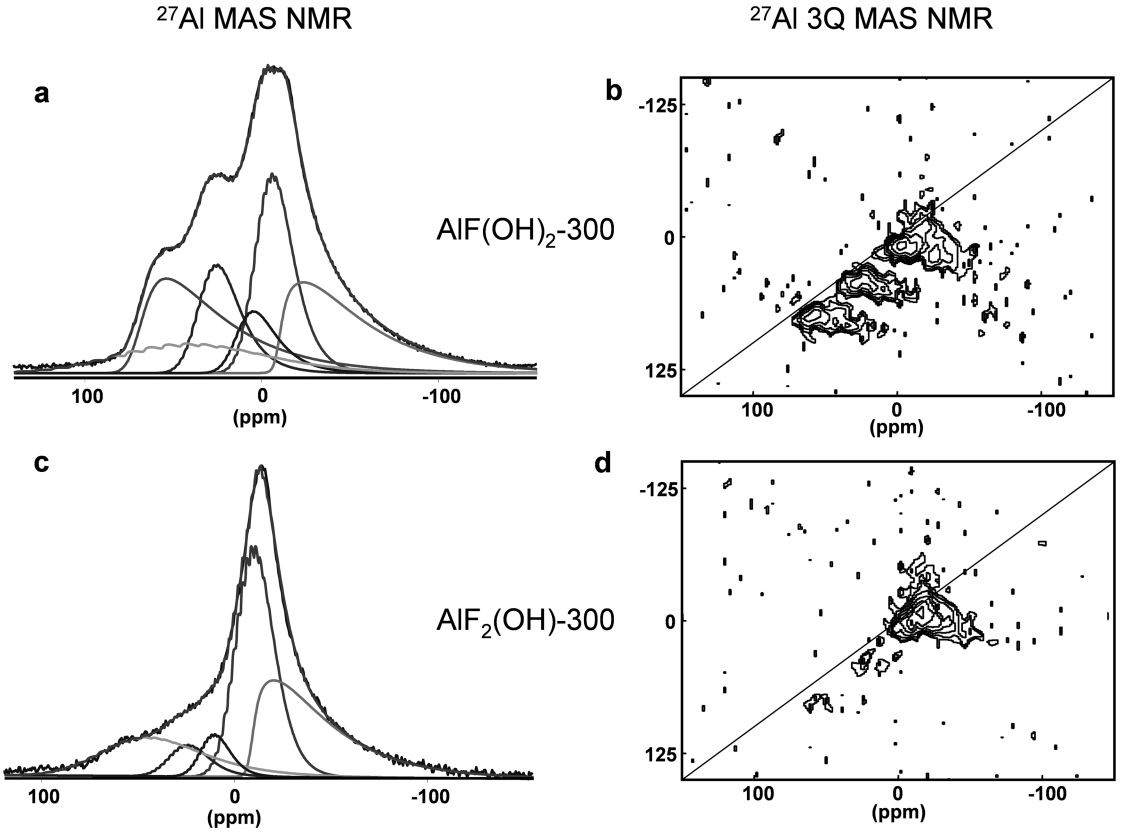

Figure 4. ^{27}Al MAS NMR spectra (central transitions) along with decompositions and ^{27}Al 3Q MAS NMR spectra of $AlF(OH)_2$-300 (a and b) and $AlF_2(OH)$-300 (c and d). All spectra were recorded at rotation frequencies of 25 kHz. The diagonal represents the chemical shift axis.

of this signal illustrates the dismutation of $AlF(OH)_2$-500 into aluminum oxide-hydroxide fluoride phases with less and more fluorine. With the loss of OH groups, the structural unit is shrinking and therefore the charge density around fluorine is increasing. This may lead to the observed shift of the signal maximum to lower binding energy like in AlF_3. The result of the O 1s measurement is in line with the Al 2p and F 1s spectra of $AlF(OH)_2$-500. The content of AlOOH-like oxygen increases because of the formation of $AlO(OH)_xF_y$ caused by dehydration. A second oxygen species at higher binding energy is compatible with strongly polarized OH groups like in $AlF_2(OH)$ (see Figure 3).

The broadened Al 2p spectrum of $AlF_2(OH)$-300 (Figure 3) can again be reproduced with one single line, which is, compared to $AlF(OH)_2$-300, shifted to higher binding energies indicating the increased fluorine content in the sample caused by the partial condensation of OH groups forming H_2O and residual oxygen. The broad F 1s spectrum of AlF_2OH-300 can in this case be fitted with two lines, indicating a bimodal distribution may exist. The signal at higher binding energy is similar to the signal of α-AlF_3. The component at lower binding energies suggests that electron donation from geminal OH groups enhances the charge density of some of the fluorine species. The O 1s spectrum of $AlF_2(OH)$-300 shows large amounts of moderately polarized OH-groups. However, there is also the generation of AlFO(OH) species visible. Further calcination leads to a dismutation of $AlF_2(OH)$-500 into oxygen rich $AlO(OH)_xF_y$ and fluorine rich $AlF_2O_x(OH)_y$ phases. Because of the highest relative fluorine content, $AlF_2(OH)$-500 is the maximum of the F 1s spectrum and has the lowest binding energy value. The O 1s spectrum shows dismutation and a strong reduction in the emission intensity from polarized OH groups, explainable with an almost complete dehydration. The increase of the signal at lower binding energy is due to the generation of O(H) in AlO_6 units like in a AlO(OH) or Al_2O_3, whereas the signal at high binding energies depicts the building of AlFO(OH) species with high fluorine content.

Since XPS is a surface analysis method, we used MAS NMR spectroscopy to analyze the bulk. In Figure 4, the ^{27}Al MAS NMR spectra (central lines) of $AlF(OH)_2$-300 (Figure 4a) and $AlF_2(OH)$-300 (Figure 4c) are shown. The ^{27}Al MAS NMR spectrum of $AlF(OH)_2$-300 is very similar to the spectrum of $AlF(OH)_2$-180 (Figure 1a in ref 11) and also consists of at least three central signals with maxima at -7 ppm (due to AlF_xO_{6-x} units),[1,11,27] 26 ppm (due to AlF_xO_{5-x} units),[1,11,27,28] and 54 ppm (due to AlF_xO_{4-x} units).[1,11,27,28] The dehydration of $AlF(OH)_2$ at 300 °C leads, compared with $AlF(OH)_2$-180 (Figure 1a in ref 11), to an intensity increase of the signals at 54 and 26 ppm. As mentioned before, Vasiliev et al. reported the structure of crystalline orthorhombic aluminum oxide fluoride, which consists of octahedral and tetrahedral coordinated aluminum with a mixed fluorine/oxygen coordination.[13] Therefore the existence of 4-fold coordinated

(27) König, R.; Scholz, G.; Pawlik, A.; Jäger, C.; van Rossum, B.; Oschkinat, H.; Kemnitz, E. *J. Phys. Chem. C* **2008**, *112*, 15708.
(28) König, R.; Scholz, G.; Pawlik, A.; Jäger, C.; van Rossum, B.; Kemnitz, E. *J. Phys. Chem. C* **2009**, *113*, 15576–15585.

aluminum species in $AlF(OH)_2$-300 is not surprising. The ^{27}Al MAS NMR spectrum of $AlF_2(OH)$-300 (Figure 4c) is dominated by a strong asymmetric signal at −14 ppm (AlF_5O).[1,11,27,28] The high-field shift of the central signal is caused by the higher fluorine content of $AlF_2(OH)$-300 in contrast to $AlF(OH)_2$-300. The slight shoulders in the low-field part of the spectrum denote the existence of further Al species with coordination numbers of five (signal at ~26 ppm, AlF_xO_{5-x})[1,11,27,28] and four (signal at ~57 ppm, AlF_xO_{4-x}).[1,11,27,28] The intensity of these signals is, compared to $AlF(OH)_2$-300, strongly reduced. Obviously, the higher fluorine content leads to an increase of the number of octahedrally coordinated Al species. The spectra of $AlF_2(OH)$-180 (Figure 1b in[11]) and $AlF_2(OH)$-300 are very similar. Even the intensities of the shoulders at about 26 and 57 ppm are comparable. However, the dehydration leads to a slight decrease of the fwhm in the spectrum of $AlF_2(OH)$-300 and therefore to an increase of the structural order. This finding is in line with the results of FT-IR spectroscopy. All recorded signals are broad and asymmetric originating not only from superimpositions of Al sites different in their coordination number (4-, 5-, and 6-fold coordinated Al species) but also different in their chemical environment (fluorine, hydroxide, and oxide coordination). Taking into account such distributions and superimpositions, a deconvolution of the experimental spectra (Figure 4a,c) is not possible without many uncertainties from single pulse spectra. Therefore, 3Q MAS experiments were performed (Figure 4b,d) to facilitate a discrimination between different sites and to obtain essential parameters for the simulation. The sheared ^{27}Al 3Q MAS NMR spectra of $AlF(OH)_2$-300 (Figure 4b) and $AlF_2(OH)$-300 (Figure 4d) are shown. For both phases, at least three different Al sites can be distinguished, which is much more clear for $AlF(OH)_2$ (Figure 4b). For these resonances it is possible to determine the centers of gravity from the 3Q MAS spectra characterized by the isotropic shift δ_{3QMAS} (F1) and the anisotropic shift δ_{MAS} (F2). The corresponding values are listed in Table 2. With eqs 2−4, they can be used for estimating the quadrupolar product $\nu_{Q\eta}$ and the isotropic chemical shift δ_{iso} for each site.

$$P_Q = \frac{\sqrt{85}}{900}\nu_0\sqrt{\delta_{3QMAS} - \delta_{MAS AS}} \quad (2)$$

$$\nu_{Q\eta} = \frac{3P_Q}{(2I(2I-1))} \quad (3)$$

$$\delta_{iso} = \frac{17}{27}\delta_{3QMAS} + \frac{10}{27}\delta_{MAS} \quad (4)$$

The parameters of three sites, Al6-1 (AlX-Y; X is the coordination number and Y indicates the different species), Al5-1, and Al4-1, can be determined very clearly from 3Q MAS (see Table 2). The derived isotropic chemical shifts (δ_{iso}) (Table 2) can be assigned to 6-fold, 5-fold, and 4-fold coordinated Al species. However, the simulation of the single pulse spectra with only these three sites and using Czjzek-distributions was not successful. As also indicated by the shape of the spinning side bands (not shown here) and the strong asymmetry, an extension in the 3Q MAS spectra and further Al sites could be identified, i.e., a further three sites were added for $AlF(OH)_2$-300 and two additional sites were added for $AlF_2(OH)$-300, respectively (see Table 2). Because of uncertainties for the assignment of the latter in the 3Q MAS spectra, their parameters of simulation show slight deviations. Finally six ($AlF(OH)_2$-300) or five (AlF_2OH-300) different Al sites were included into the simulation for the samples. The respective decomposition is enclosed in part a ($AlF(OH)_2$-300) and part c ($AlF_2(OH)$-300) of Figure 4, giving satisfactorily fits of the experimental 1D spectra.

A successful deconvolution of the spectrum of $AlF(OH)_2$-300 (Figure 4a) results in six lines. Three lines (Al6-1, Al6-2, and Al6-3) have their maxima in a region between $\delta_{(iso)} \approx -10$ and 15 ppm and can therefore be assigned to 6-fold coordinated Al sites in a mixed oxygen/fluorine environment.[1,27] With increasing fluorine content of the AlF_xO_{6-x} octahedra, the signal maximum is shifted to higher field. For this reason, the line of Al6-2 (Figure 4a, $\delta_{iso} = -9.3$ ppm) represents the highest fluorinated AlF_xO_{6-x} octahedra with $x \geq 4$.[11,27] The position of the second intense line (Figure 4a, Al6-1) is at $\delta_{iso} = 1.8$ ppm, which is a typical value for the presence of AlF_3O_3 octahedra.[27] The peak areas of both lines are almost equal (Table 2).

The assignment of the third line (Figure 4a, Al6-3) with its position at 14.1 ppm is ambiguous. This line could either be assigned to 6-fold oxygen coordinated aluminum similar to corundum[29] or to 6-fold coordinated AlF_xO_{6-x} with $x = 1$. The XPS measurements (Figure 3) suggest the existence of 6-fold coordinated AlF_1O_5 because of the absence of typical signals of AlO_6 like in boehmite or corundum. According to König et al.,[28] the line at $\delta_{iso} = 34.8$ ppm (Figure 4a, Al5-1) can be attributed to 5-fold coordinated AlF_xO_{5-x} or possibly 4-fold coordinated AlF_xO_{4-x} with $x \leq 3$.[28] The existence of these aluminum species shows the high degree of structural disturbance caused by sol−gel synthesis and by thermal dehydration of the samples.[11] The last two lines with δ_{iso} values at 66.5 and 70.3 ppm (Figure 4a, Al4-2 and Al4-1) can be clearly assigned to 4-fold coordinated AlF_xO_{4-x} ($x = 0-4$) species.[28,30] The crystal structure of AlFO reported by Vasiliev et al. consists of AlF_xO_{6-x} octahedra and of AlF_xO_{4-x} tetrahedra.[13] Therefore, the existence of 4-fold coordinated aluminum species and the high peak areas of their signals (Table 2) are not astonishing even though our samples are amorphous.

The deconvolution of the spectrum of $AlF_2(OH)$-300 (Figure 4c) results in only five lines. Again, three lines (Al6-1, Al6-2, and Al6-3) have their maxima in a region between $\delta_{(iso)} \approx -10$ and 15 ppm and can therefore be assigned to 6-fold coordinated Al sites.[1,27] The line of Al6-2 (Figure 4c, $\delta_{iso} = -8.6$ ppm) represents the highest fluorinated AlF_xO_{6-x} octahedra with $x \geq 4$.[11,27] The second intense line (Figure 4c, Al6-1, $\delta_{iso} = -3.4$ ppm) can be assigned

(29) Dressler, M.; Nofz, M.; Malz, F.; Pauli, J.; Jäger, C.; Reinsch, S.; Scholz, G. *J. Solid State Chem.* **2007**, *180*, 2409.
(30) Abraham, A.; Prins, R.; van Bokhoven, J. A.; van Eck, E. R. H.; Kentgens, A. P. M. *J. Phys. Chem. B* **2006**, *110*, 6553.

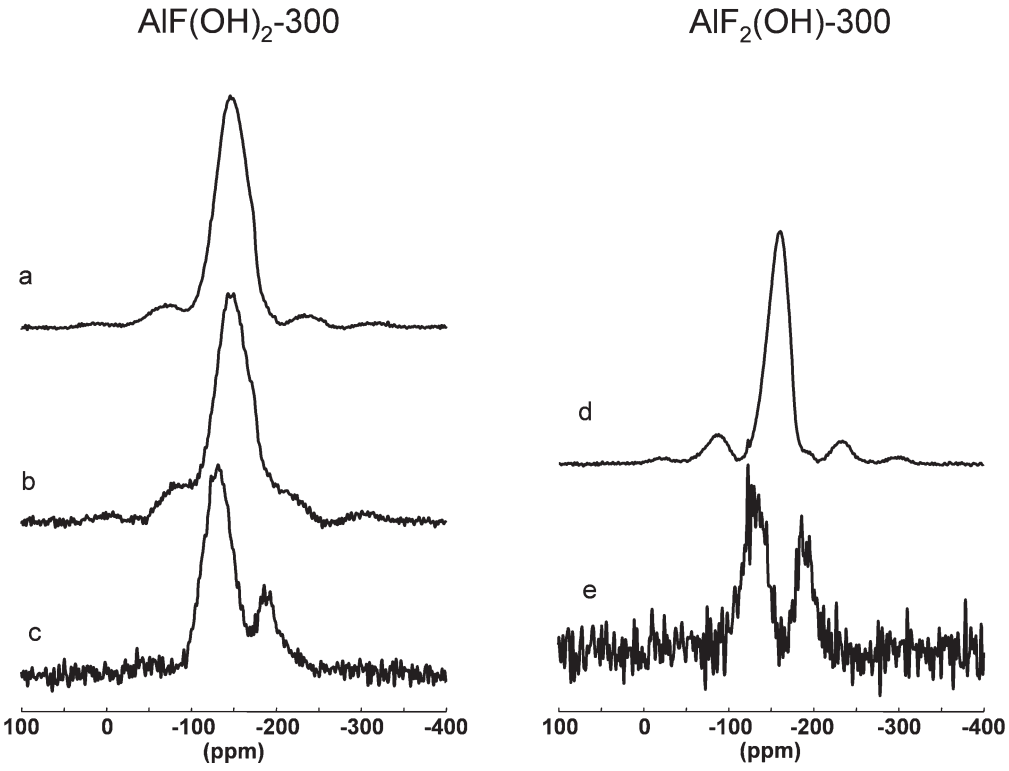

Figure 5. ^{19}F MAS NMR and rotor synchronized ^{19}F MAS spin echo spectra of $AlF(OH)_2$-300 (a−c) and $AlF_2(OH)$-300 (d and e). Spectrum a was recorded at rotation frequency of 30 kHz, and spectra b−e were recorded at rotation frequencies of 25 kHz. The rotor synchronized echo experiments (c and e) were performed with accumulation numbers (ns) of 256 with a delay (L0) of 40 rotor periods.

to AlF_4O_2 octahedra.[27] The peak areas of both lines are almost equal but altogether higher as in the spectrum of $AlF(OH)_2$-300 (Table 2). As well as in $AlF(OH)_2$-300, the XRD pattern and XPS spectra show no hints for the existence of AlO_6 units like in corundum and therefore the line at 15.8 ppm (Figure 4c, Al6-3) can be assigned to 6-fold coordinated AlF_1O_5. A 5-fold coordinated Al site (Figure 4c, Al5-1) can be assigned with its position at 31.6 ppm, a typical value for AlF_xO_{5-x} with $x \leq 3$.[28] The line Al4-1 (δ_{iso} = 65.4 ppm) can be attributed to AlF_xO_{4-x} species.[28,30] The differences between the δ_{iso} values derived from the 3Q MAS spectrum and simulation (Table 2) are smaller than obtained for the other sample. This is due to the higher fluorine content, which leads to 76.6% of all Al-sites in 6-fold at least partial fluorine coordination. For comparison, in $AlF(OH)_2$ these are only 51.1%.

In Figure 5, the ^{19}F MAS NMR spectra (Figure 5a,b and d) and the results of ^{19}F rotor synchronized delayed echo experiments of $AlF(OH)_2$-300 (Figure 5c) and $AlF_2(OH)$-300 (Figure 5e) are shown. Both, the ^{19}F MAS NMR spectrum of $AlF(OH)_2$-300 (Figure 5a and b) and the spectrum of $AlF_2(OH)$-300 (Figure 5d) consist of extremely broad, asymmetric signals with maxima of the chemical shift at −146 ppm ($AlF(OH)_2$-300) or −161 ppm ($AlF_2(OH)$-300). On the basis of the ^{19}F−^{27}Al HETCOR spectrum (Figure 7), the signal of $AlF(OH)_2$-300 at −146 ppm can be assigned to a bridging fluorine in 6- and 5-fold coordinated Al species.[16,28,31] An estimated line width of about 14 kHz even at a spinning speed of 30 kHz for $AlF(OH)_2$-300 cover possible different fluorine species. Delayed rotor-synchronized echo experiments, utilizing different spin−spin relaxation times (T2) of the particular species were performed to find out and to resolve different fluorine sites. After 40 rotor periods before echo detection, the spectrum of $AlF(OH)_2$-300 (Figure 5c) shows two well separated signals at −131 ppm and at −186 ppm, respectively, the first one with higher intensity. The more intense signal in the low field part of the spectrum depicts a bridging fluorine in the 5-fold coordinated Al species.[28] The signal at −186 ppm is typical for terminal fluorine sites in AlF_xO_{5-x} species with x = 2−5.[28]

Similar results were obtained for $AlF_2(OH)$-300. The high field shift of the main ^{19}F signal is compared to $AlF(OH)_2$-300 caused by the increased fluorine content of the sample.[11,31] Here too, the asymmetry of this spectrum indicates the superposition of different 6-, 5-, or 4-fold fluorine coordinated Al sites. The shape of the spectrum of the delayed rotor-synchronized echo experiment of $AlF_2(OH)$-300 (Figure 5e) is very similar to $AlF(OH)_2$-300, but the signal-to-noise ratio is worse choosing the same experimental conditions. This is due to a fewer number of species with longer spin−spin relaxation times, and therefore the structural order of $AlF(OH)_2$-300 is higher as in $AlF_2(OH)$-300. An assignment of the fluorine signals is highly speculative as long as it is not known at which kind of Al site (4-, 5-, or 6-fold coordinated Al sites) they are located. Again, two signals at −131 and −186 ppm are visible, indicating bridging and terminal fluorine. According to ref 28, both signals can be attributed to AlF_xO_{5-x} units (x = 2−5). The appearance of ^{19}F echo signals for terminal fluorine sites

(31) König, R.; Scholz, G.; Bertram, R.; Kemnitz, E. *J. Fluorine Chem.* **2008**, *129*, 598.

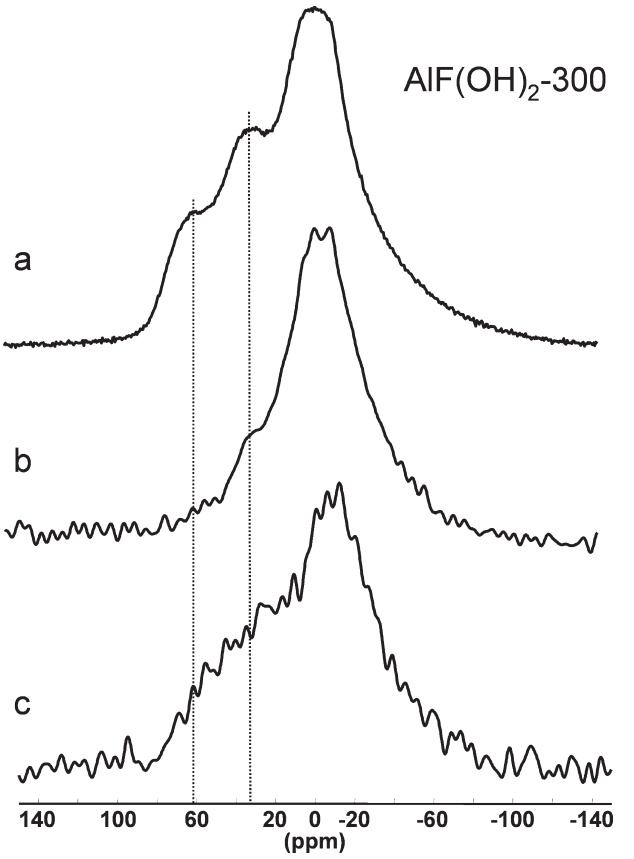

Figure 6. ^{27}Al MAS (a) and ^{19}F−^{27}Al CP MAS NMR spectra (b and c) of AlF(OH)$_2$-300 with different CP matching conditions. All spectra were recorded at rotation frequencies of 25 kHz; (b) attenuation 32 dB, ns, 12 288; (c) attenuation, 22 dB; ns, 15 416.

in both samples affirms the results of the F 1s XPS measurements, which also give strong hints for the existence of terminal fluorine sites. For these reasons, the terminal F sites are located at the surface[32] and in the bulk as a consequence of poorly cross-linked Al polyhedra.

In Figure 6, the ^{27}Al MAS NMR spectrum (Figure 6a) and the ^{19}F−^{27}Al CP MAS NMR spectra of AlF(OH)$_2$-300 with different attenuations (Figure 6, 32 dB (b) and 22 dB (c)) are shown. Because of the varying aluminum environments, the power of the polarization transfer is different for the individual species. The CP spectra evidence that all the Al sites (6-, 5-, and 4-fold coordinated, see Table 2) are at least partially bonded to fluorine. Additionally, a ^{19}F−^{27}Al HETCOR MAS NMR measurement of AlF(OH)$_2$-300 was performed (Figure 7). With this 2D-technique, it is in principle possible to assign different Al and F sites to each other. It is visible that the central transition of the ^{19}F spectrum (Figure 5a) is built by fluorine in 6- and 5-fold coordinated aluminum.[31] Because of the attenuation of 32 dB chosen for the HETCOR experiment, the 6-fold coordinated Al sites are overestimated and the 4-fold coordinated aluminum species are not visible (see Figure 6b).

(32) Makarowicz, A.; Bailey, C. L.; Weiher, N.; Kemnitz, E.; Schroeder, S. L. M.; Mukhopadhyay, S.; Wander, A.; Searle, B. G.; Harrison, N. M. *Phys. Chem. Chem. Phys.* **2009**, *11*, 5664.

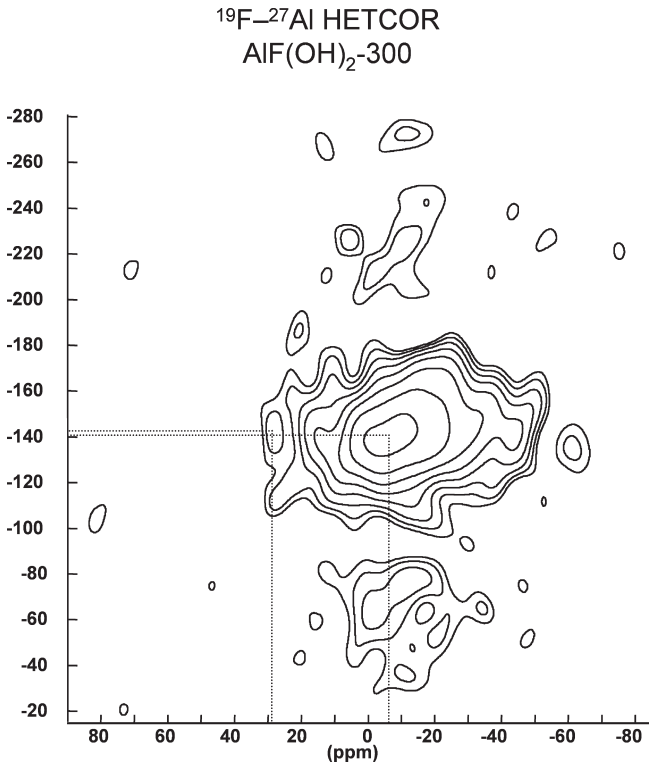

Figure 7. ^{19}F−^{27}Al HETCOR MAS NMR spectrum of AlF(OH)$_2$-300 (attenuation for the CP match, 32 dB).

Conclusions

In the present paper, the structure and properties of aluminum oxide-hydroxide fluorides were investigated. It was shown that the thermal treatment of amorphous aluminum hydroxide fluorides leads to a partial dehydration of the samples forming aluminum oxide-hydroxide fluorides. These X-ray amorphous compounds exhibit high surface areas and strong (Lewis) acid centers. FT-IR measurements evidenced the existence of Al−O, Al−OH, and Al−F bonds in the samples along with the typical stretching and deformation vibrations of water molecules. These results were confirmed by XPS measurements of the aluminum oxide-hydroxide fluorides. With increasing temperature, the samples begin to dismutate into fluorine rich and fluorine depleted phases. The analysis of 3Q MAS NMR spectra allowed a subsequent deconvolution of the ^{27}Al MAS NMR spectra into different 6-, 5-, and 4-fold coordinated aluminum species. It turns out that the different fluorine contents of the samples widely influence the relative content of 4-, 5-, and 6-fold coordinated aluminum species. The number of 6-fold coordinated Al species increases with increasing fluorine content in the sample, i.e., 51.1% in AlF(OH)$_2$-300 and 76.6% in AlF$_2$OH-300, respectively. The relative amount of 4- and 6-fold coordinated Al sites in AlF(OH)$_2$-300 is similar to that found for crystalline AlFO very recently.[13] The evidence of high structural disturbance of the samples was provided by ^{19}F rotor synchronized echo experiments. The obtained signals at −186 and −131 ppm stand for terminal F sites and bridging fluorine in a mixed 5- or 6-fold coordinated Al environment. Especially, these terminal

F sites should be responsible for the unusual high binding energies of the F 1s XPS spectra of $AlF(OH)_2$-300. Finally, it could be shown that fluorine is bonded to every existing Al species in the samples. Summation of all the findings shows that gentle dehydration of aluminum hydroxide fluorides leads to aluminum oxide-hydroxide fluorides and not to a decomposition into aluminum oxides and aluminum fluorides.

Acknowledgment. The DFG (Grant Ke 489/22-2) is acknowledged for financial support. Dr. A. Zehl and U. Kätel are acknowledged for the elemental analysis, S. Bässler for the F-determination, and Dr. M. Feist (all Humboldt-Universität zu Berlin, Institut für Chemie) for performing the thermoanalytical measurements. Dr. R. Bertram (Leibnitz Institut für Kristallzüchtung) is acknowledged for the determination of the Al-content of the samples.